



Fe-Ca interactions in Fe-based/CaO catalyst/sorbent for CO₂ sorption and hydrogen production from toluene steam reforming

I. Zamboni, C. Courson*, A. Kiennemann

Institut de Chimie et Procédés pour l'Energie, l'Environnement et la Santé, Equipe "Energie et Carburants pour un Environnement Durable", UMR CNRS 7515, ECPM-Université de Strasbourg, 25 rue Becquerel, 67087 Strasbourg Cedex 2, France

ARTICLE INFO

Article history:

Received 7 July 2016
Received in revised form 4 October 2016
Accepted 8 October 2016
Available online 11 October 2016

Keywords:

Toluene steam reforming
CO₂ sorption
Iron oxides
CaO

ABSTRACT

After biomass gasification, tar can be removed by steam reforming and additional hydrogen production. This latter can be enhanced by CO₂ sorption using the global process known as sorption enhanced hydrogen production (SEHP). Toluene was studied as tar model compound and its reforming was carried out at a compromise temperature (700 °C) to permit simultaneous activation of iron based catalyst and CO₂ sorption on CaO based sorbent.

Fe-Ca interactions on Fe-based/CaO catalyst/sorbent performances occur during steam reforming of toluene. In order to determine the specific conditions for the formation of the different iron species, Fe-based/CaO bi-functional materials have been prepared following three different methods with various calcium and iron precursors. The characterizations (XRD, Mossbauer spectroscopy, TGA, TPR, SEM, and BET/BHJ) performed before and after steam reforming of toluene provide information about the evolution of the iron species and Fe-Ca interactions during catalytic tests. The results suggest that the activity of Fe/CaO materials depends not only on the presence of Fe₂O₃ but also on the stability of the interactions between iron and calcium under reaction conditions.

The bi-functional material prepared from iron acetate and calcium acetate by mechanical mixing (FeAc/CaO (M)) has properties (large specific surface area, appropriate sorption capacity at 700 °C, and the lowest deactivation) that play an important role for CO₂ capture. Moreover, the presence of the α-Fe₂O₃ phase, precursor of the active phase in steam reforming of tar, reducible at 700 °C, intervenes in the hydrogen production rate by enhancing the Water Gas Shift reaction. Finally, its higher availability of iron (Fe₂O₃) limit the selectivity towards undesirable products such as benzene.

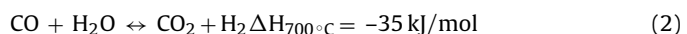
© 2016 Elsevier B.V. All rights reserved.

1. Introduction

Hydrogen production from biomass is a promising environmental and economic method of energy supply [1]. The thermo-chemical conversion of biomass by a gasification process produces a synthesis gas (syngas) that not only contains H₂ and CO but also CO₂, CH₄ and tar. Tar is a mixture of polycyclic aromatic hydrocarbons which is harmful for a biomass process and for syngas applications. To minimize its impact, tar can be converted into valuable products (H₂ and CO) by catalytic steam reforming of aromatics [2–5] (Eq. (1) for toluene used as a tar model compound).



Recently, iron based catalysts have gained an interesting place among catalysts for tar conversion [6–9] and metallic iron is the efficient phase for tar cracking [10–12]. Moreover, magnetite (Fe₃O₄) activity has been proved in Water Gas Shift (Eq. (2)) reaction (WGS) at high temperature [13]. Compared to nickel, the use of iron minimizes the cost and toxicity of the process.

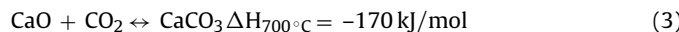


Uddin et al. [14] observed that iron oxides, such as hematite (Fe₂O₃), promote tar gasification at 600 °C, while magnetite phase (Fe₃O₄) affects the composition of the biomass gasification gaseous products. When the Fe₃O₄ phase is present the production of H₂ and CO₂ increases and CO production decreases. This shows the activity of such a phase in the Water Gas Shift reaction. If CO₂ partial pressure in the gas product is reduced the WGS reaction is shifted to hydrogen production [15]. So, the efficiency of tar steam reforming might be improved by CO₂ sorption using the global process known as sorption enhanced hydrogen production (SEHP).

* Corresponding author.

E-mail address: claire.courson@unistra.fr (C. Courson).

CaO sorbents are widely used in CO₂ sorption due to their high carbonation capacity and decarbonation in a wide operating temperature range between 500 °C and 800 °C [16]. Sorption on CaO (Eq. (3)) helps to partly balance the endothermicity of the steam reforming reaction (Eq. (1)).



A bi-functional material with catalytic activity in steam reforming of tar and CO₂ sorption capacity can be a Fe-based/CaO catalyst/sorbent. However, in the temperature range of CO₂ sorption and steam reforming (700 °C–850 °C), the activity of iron species and CaO can be limited by the presence of strong Fe-Ca interactions as a consequence of the Ca₂Fe₂O₅ phase (srebrodolite) formation during catalyst preparation [6].

Huang et al. [17] studied, in the biomass gasification at 660 °C, a Fe/CaO catalyst in which CaO and Ca₂Fe₂O₅ were the main phases observed. The decrease in tar production has been attributed to a synergy between the two phases, which avoids the deactivation of CaO by tar and promotes biomass gasification and hydrogen production. The latter were not attributed to iron present in the Ca₂Fe₂O₅ structure due to its unavailability at low gasification temperature.

In the Ca₂Fe₂O₅ phase, iron is both octahedrally and tetrahedrally coordinated by oxygen and the structure consists in alternating parallel iron-oxygen octahedra and tetrahedra with calcium atoms in holes between the polyhedra of nine oxygen atoms [18]. This slight shift of the iron atoms from the cubic perovskite structure ABO₃ creates oxygen vacancies (1/6) [19,20] that facilitate the mobility of oxygen.

These oxygen vacancies can provide the catalytic character of the Ca₂Fe₂O₅ phase in deep oxidation of carbon monoxide [21], oxidation of volatile organic compounds [22] and in direct decomposition of NOx in exhaust streams [23]. Although this structure may have a catalytic capability, there is no evidence of the behaviour of this phase during the steam reforming of tar.

This work focuses on the understanding of the Fe-Ca interactions on Fe-based/CaO catalyst/sorbent performances in steam reforming of tar (Eq. (1)) and in CO₂ sorption (Eq. (3)). In order to determine the specific conditions for the formation of the different iron species, Fe-based/CaO bi-functional materials have been prepared following three different methods with various calcium and iron precursors. Sorption properties and activity in steam reforming of toluene were evaluated at 700 °C, maximum temperature imposed by the thermodynamic constraints of the reaction between CO₂ and CaO at ambient pressure [24]. The characterizations performed before (XRD, Mossbauer spectroscopy, TGA, TPR, SEM, and BET/BHJ) and after (XRD, Mossbauer spectroscopy, and TPR) steam reforming of toluene provide information about the evolution of the iron species and Fe-Ca interactions during catalytic tests.

2. Materials and methods

2.1. Material preparation

Calcium acetate monohydrate (Ca(C₂H₃O₂)₂·H₂O) reagent-grade purchased from Sigma Aldrich was used as the calcium precursor. The iron precursor's salts used were iron (II) acetate anhydrous (Fe(C₂H₃O₂)₂ noted FeAc) and iron (III) nitrate ((Fe(NO₃)₃)·9H₂O noted FeN) purchased from Alfa Aesar and Acros Organics, respectively.

CaO was obtained by calcination of calcium acetate monohydrated at 750 °C (3 °C/min then 4 h). Impregnation (noted I), mechanical mixing (noted M) and pseudo sol-gel (noted S) methods, following the instructions previously described [25], permitted

the obtaining of Fe-based/CaO bi-functional materials containing 10 wt% of iron at a single calcination temperature (750 °C). All the samples were sieved between 125 µm and 250 µm.

The Fe-based/CaO bi-functional materials were summarized in Table 1.

2.2. Structural characterization

Structural characterization of bi-functional materials was performed by X-ray diffraction (XRD), Mossbauer spectroscopy, and temperature programmed reduction (TPR).

2.2.1. X-ray diffraction (XRD)

X-ray diffraction patterns were acquired with a Brucker AXS-D8 Advanced using CuK radiation ($\lambda = 1.5418 \text{ \AA}$) to identify the crystalline phases in a 2θ range of 20°–70° (step = 0.0158°, time per step = 1 s). The diffraction spectra have been indexed by comparison with the JCPDS files (Joint Committee on Powder Diffraction Standards) and the CaO lattice parameter determined. Crystallites sizes of the different phases were evaluated by Debye-Scherrer equation from the width at half-height (FWHM) of the more intense and better deconvoluted ray of each phase.

2.2.2. Mossbauer spectroscopy

The Mossbauer spectra measurements were carried out in transmission mode with ⁵⁷Co diffused into an Rh matrix as a source moving at a constant acceleration. The spectrometer (Wissel) was calibrated by means of a α -Fe foil standard, and the isomer shift was expressed with respect to this standard at 293 K. The fitting of the spectra was performed using the NORMOS program.

2.2.3. Thermogravimetric analysis of precursors and bi-functional materials formation

Thermogravimetric analysis under air follows the decomposition of the sample in the actual conditions of calcination by measuring of the mass (and its speed variation) as a function of temperature. The equipment used is a thermobalance TGA Q5000 IR by TA Instruments. Sample mass is around 20 mg and air flow is about 20 mL/min.

2.2.4. Temperature programmed reduction (TPR)

The temperature programmed reduction was performed with a Micromeritics Autochem II Chemisorption Analyzer. Firstly, a precise amount of the sample (50 to 100 mg) was heated under Ar up to 750 °C (15 °C/min). Then, to clean it, this was maintained 30 min at 750 °C. Next, it was cooled to room temperature. The sample was reduced by a 10%H₂/Ar flow during an increase in temperature of up to 1000 °C (15 °C/min) and a plateau of 30 min, at the same temperature. The hydrogen consumption of the samples was followed by a thermal conductivity detector (TCD) until a return to the baseline.

2.3. Textural characterization

For surface characterization, techniques such as scanning electron microscopy (SEM) and nitrogen adsorption associated with BET and BJH methods were used.

2.3.1. Scanning electron microscopy (SEM)

The scanning electron microscopy (SEM) was performed on a JEOL JSM-6700F apparatus. Prior to the analysis, samples were coated with a conductive film of carbon to avoid charging effect. The analyses were performed using an accelerating voltage between 3 and 9 kV.

Table 1

Synthesised bi-functional materials Fe-based/CaO.

Iron precursor	Synthesis method		
	Impregnation (I)	Mechanical mixing (M)	Pseudo sol-gel (S)
Iron (II) acetate anhydrous (FeAc)	FeAc/CaO (I)	FeAc/CaO (M)	FeAc/CaO (S)
Iron (III) nitrate (FeN).	–	FeN/CaO (M)	–

Table 2CaO lattice parameter and CaO, $\text{Ca}_2\text{Fe}_2\text{O}_5$ and Fe_2O_3 crystallites size of CaO from calcium acetate, Fe_2O_3 from iron acetate and bi-functional materials.

Bi-functional materials	CaO crystallites size (nm) ± 1 nm	$\text{Ca}_2\text{Fe}_2\text{O}_5$ crystallites size (nm) ± 1 nm	Fe_2O_3 crystallites size (nm) ± 1 nm
CaO	36	–	–
FeAc.	–	–	47
FeAc/CaO (I)	39	35	–
FeAc/CaO (S)	38	40	–
FeAc/CaO (M)	36	–	39
FeN/CaO (M)	38	22	29

2.3.2. Nitrogen adsorption (BET and BJH methods)

BET and BJH methods were based on nitrogen adsorption-desorption measurements at -196°C (77 K) using a CoulterSA3100 instrument. BET was used to determine the specific surface area of materials while BJH was used to determine the values of pore volume and pore size.

2.4. Sorption properties

Sorption tests and thermogravimetric analysis (carbonation-calcination cycles) were performed at 700°C to evaluate the sorption capacity of the bi-functional materials and the stability of their sorption capacity during carbonation-calcination cycles.

2.4.1. Sorbent capacity

The sorption tests were carried out with 100 mg of bi-functional materials by utilising a fixed bed reactor (6 mm of inner diameter). During the first step, the material was heated up to 800°C under helium in order to eliminate humidity and CO_2 molecules. Afterwards, the temperature was fixed at 700°C and the CO_2 sorption step (1 h) was then started with a total flow of 3 L/h containing CO_2 (10 vol.%) in helium. Desorption was performed under He atmosphere (3 L/h) during a temperature increase from 700°C until 800°C with a heating rate of $5^\circ\text{C}/\text{min}$ to carry out the desorption until the total released of CO_2 . To assure the maximum desorption of CO_2 and to minimize sintering, the maximum temperature chosen for the desorption step was 800°C . The sorption and desorption steps were followed by a thermal conductivity detector (TCD). The total desorption of CO_2 is then equivalent to the total CO_2 that could be captured during the sorption step.

2.4.2. Sorption stability

In order to determine CO_2 sorption stability, carbonation and decarbonation were performed with a thermogravimetric analyser (TGA Q5000, TA Instruments). Thermogravimetric analysis was carried out in the previously mentioned conditions to determinate the sorption capacity. However, the initial weight sample was between 5 mg and 10 mg and the total flow was 0.3 L/h, according to TGA equipment characteristics.

2.5. Catalytic test

Catalytic activity was evaluated at 700°C in a fixed bed reactor by the steam reforming of toluene as the tar removal model reaction. The fixed bed quartz reactor (inner diameter 8 mm) containing bi-functional materials (100 mg), supported by quartz wool, was placed in a furnace in which the heating is monitored by a ther-

mocouple. Using two independent channels from the HPLC pumps, water and toluene were introduced into a vaporization furnace (250°C) and then carried to the reactor by a flow (total flow of 3 L/h) containing a mixture (95/5) of argon (carrier gas) and nitrogen (internal standard) (GHSV: 5968 h^{-1}). Toluene concentration (10 g/Nm³) was chosen in order to perform catalytic tests in conditions similar to those observed in a biomass fluidized bed gasifier (about 2–10 g/Nm³) [26]. Stoichiometric $\text{H}_2\text{O}/\text{C}_7\text{H}_8$ ratio (14/1) was established according to Eq. (4), herein, steam reforming and Water Gas Shift reaction are involved (Eqs. (1) and (2)).



Then, the gas mixture consists of 0.13 mL/min of toluene (0.27 vol.%), 1.86 mL/min of H_2O (3.72 vol.%) and 48 mL/min of Ar-N₂. According to these conditions, the S/C ratio is around 2.

The catalytic tests were carried out for 4 h at 700°C . The gas leaving the reactor was continuously analysed by three gas chromatographs. Delsi Instruments Di200 and Agilent 7890A gas chromatographs equipped with TCD were used to analyse CO_2 , H_2 , CO, CH_4 , N₂. A Varian star 3400 CX gas chromatograph equipped with FID detector was employed to quantify heavy molecules such as toluene, benzene and C_xH_y.

These results associated to the use of internal standard (N₂) permit the calculating of the hydrogen production rate (V_{H_2}) and carbon dioxide production rate (V_{CO_2}) expressed in H_2 or CO_2 moles per hour and per gram of catalyst ($\text{mol h}^{-1} \text{g}_{\text{cata}}^{-1}$), selectivity towards carbonaceous compounds (%S_i with i = carbonaceous compounds) and H_2/CO_2 molar ratio.

3. Results and discussion

3.1. Structural characterization

Structural characterization permitted, firstly, the identifying of the phases present in the bi-functional materials then, secondly, the evaluating of the CaO lattice parameter and crystallites size of the various present phases and then, finally, the understanding of their formation as a function of synthesis method or metal precursor.

3.1.1. X-ray diffraction

The diffractograms of the bi-functional materials prepared by the three synthesis methods with various iron precursors are presented Fig. 1.

XRD diffraction patterns show the presence of three phases, i.e. calcium oxide, hematite ($\alpha\text{-Fe}_2\text{O}_3$) and srebrodolskite ($\text{Ca}_2\text{Fe}_2\text{O}_5$). The calcium oxide phase is present regardless of the method and of the iron precursor used.

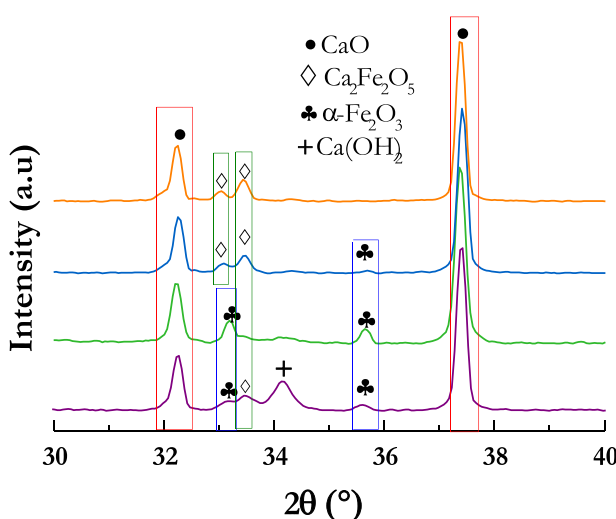


Fig. 1. XRD patterns of (—) FeAc/CaO (I), (—) FeAc/CaO (S), (—) FeAc/CaO (M) and (—) FeN/CaO (M).

With the acetate iron precursor, the impregnation method (FeAc/CaO (I)) promotes the formation of the $\text{Ca}_2\text{Fe}_2\text{O}_5$ mixed phase, the sol-gel method (FeAc/CaO (S)) allows the formation of $\text{Ca}_2\text{Fe}_2\text{O}_5$ and hematite, and the mechanical mixing (FeAc/CaO (M)) promotes the formation of $\alpha\text{-Fe}_2\text{O}_3$ (hematite) to the detriment of $\text{Ca}_2\text{Fe}_2\text{O}_5$. This confirms that the use of soft methods (impregnation and sol-gel) promotes stronger interactions between the iron phase and the sorbent.

However, with the iron nitrate precursor (FeN/CaO (M)), $\text{Ca}_2\text{Fe}_2\text{O}_5$ formation is more favourable than with iron acetate (FeAc/CaO (M)) which suggests that the decomposition of acetate decreases strong sorbent-metal interactions.

The lattice parameter (4.8 \AA) is the same in the bi-functional materials as that for CaO. Then, no solid solution is formed between CaO and an iron phase. The crystallites size of CaO and $\text{Ca}_2\text{Fe}_2\text{O}_5$ and Fe_2O_3 is detailed in Table 2. There was a slight increase in CaO crystallite size during bi-functional materials synthesis except by the mechanical mixing of iron acetate and CaO (FeAc/CaO (M)).

The crystallite size of the $\text{Ca}_2\text{Fe}_2\text{O}_5$ phase varies according to the preparation method. By impregnation, $\text{Ca}_2\text{Fe}_2\text{O}_5$ crystallites are smaller, so better dispersed than during the pseudo sol-gel method. For the mechanical mixing of iron nitrate and CaO (FeN/CaO (M)), particles size have been evaluated at 22 nm for $\text{Ca}_2\text{Fe}_2\text{O}_5$ but with a large uncertainty due to overlapping of the main ray and a ray of $\alpha\text{-Fe}_2\text{O}_3$.

By mechanical mixing, the $\alpha\text{-Fe}_2\text{O}_3$ crystallites have a smaller size (39 nm) than that of the crystallites obtained by calcination of iron acetate precursor (47 nm). This might indicate that the presence of calcium acetate favours the dispersion of $\alpha\text{-Fe}_2\text{O}_3$ particles. However, their size after calcination of the iron nitrate precursor leads to smaller $\alpha\text{-Fe}_2\text{O}_3$ particle size (29 nm). These differences of behaviour might be explained by the knowledge of the decomposition temperature for calcium and iron precursors.

Characterizations by XRD have determined the presence of various iron phases with the same oxidation state (III). However, it is not possible to quantify each species or identify iron species present in low concentration. Mossbauer spectroscopy determines the oxidation state of these iron species and their distribution in these materials.

3.1.2. Mossbauer spectroscopy

The spectrum of FeN/CaO material, given as an example (Fig. 2), presents two sextets (sub-spectra blue and green) allocated to the mixed phase $\text{Ca}_2\text{Fe}_2\text{O}_5$. This phase represents 38% of total iron

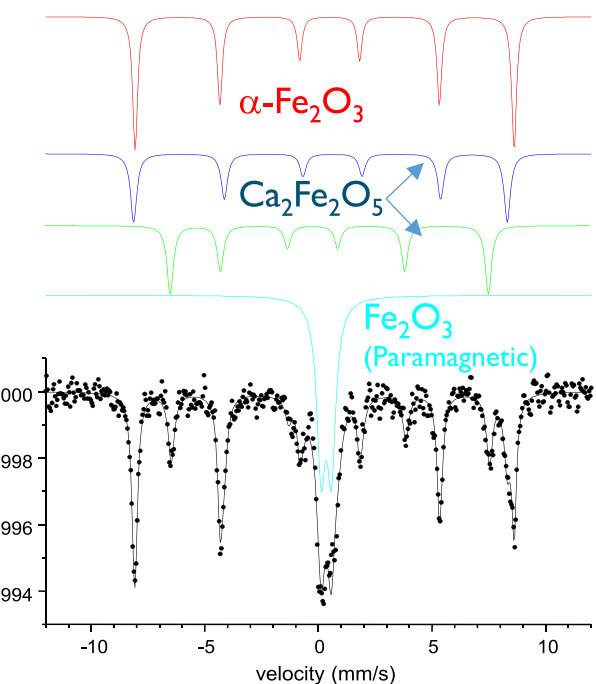


Fig. 2. Mossbauer spectra of bi-functional materials prepared by mechanical mixing from iron nitrate FeN/CaO (M).

Table 3
Iron phases and their content by ^{57}Fe Mossbauer in bi-functional materials.

Bi-functional materials	Iron distribution in the iron phases (%)	
	$\text{Ca}_2\text{Fe}_2\text{O}_5$	Fe_2O_3
FeAc/CaO (I)	94	6
FeAc/CaO (S)	77	33
FeAc/CaO (M)	12	88
FeN/CaO (M)	38	62

(Table 3). The blue sub-spectrum corresponds to Fe^{3+} in the octahedral sites and the green sub-spectrum is attributed to Fe^{3+} in the tetrahedral sites of the structure.

The red sub-spectrum is assigned to Fe^{3+} in the hematite and corresponds to 29% of total iron and the doublet (in light blue sub-spectrum) is assigned to the trivalent iron paramagnetic and is observed at 33%. The total content of Fe_2O_3 in the sample is then at 62% (Table 3).

Mossbauer spectroscopy confirms the main presence of the $\text{Ca}_2\text{Fe}_2\text{O}_5$ phase (Table 3) in the samples prepared by impregnation (I) and sol-gel (S) methods. Fe_2O_3 ($\alpha\text{-Fe}_2\text{O}_3$ and paramagnetic Fe_2O_3) is formed using mechanical mixing (M), moreover the use of iron acetate (FeAc/CaO) increases the yield of this phase regarding the samples obtained from iron nitrate (FeN/CaO). The formation of the unsuitable $\text{Ca}_2\text{Fe}_2\text{O}_5$ phase on CaO is then limited by using iron acetate and the mechanical mixing (M) method.

3.1.3. Thermogravimetric analysis of precursors and bi-functional materials formation

The mechanical mixing synthesis has been studied by thermogravimetric analysis in order to identify the formation path of $\alpha\text{-Fe}_2\text{O}_3$ (hematite) and $\text{Ca}_2\text{Fe}_2\text{O}_5$ depending of the iron precursor.

The decomposition temperature of iron nitrate (FeN) is around 150°C and that of iron acetate (FeAc) is around 260°C (Fig. 3). Iron nitrate decomposes through various processes (evaporation, hydrolysis, decomposition, and dehydroxylation) leading to iron oxide [27]. In the case of the acetate precursor, iron is in the oxidation state 2+. This involves oxidation steps which occur at the same

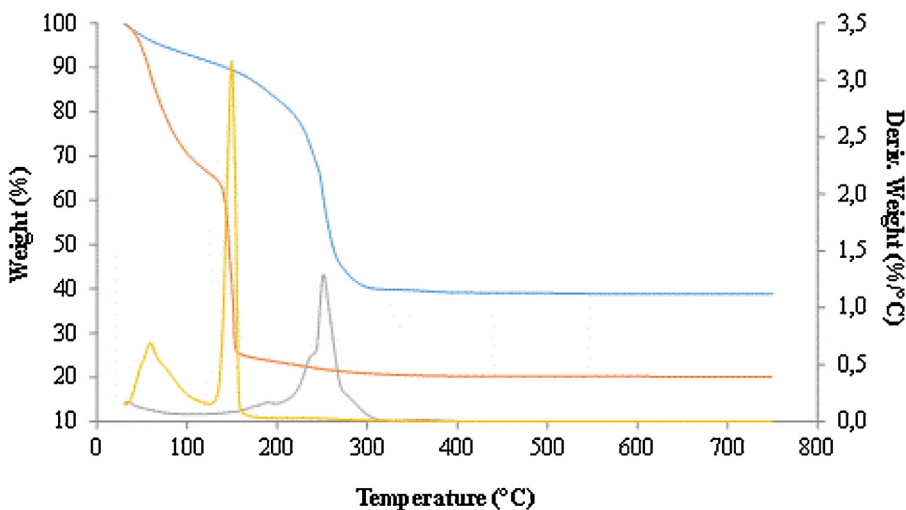


Fig. 3. TGA profiles: weight loss and derivatives of (— and —) iron nitrate and (— and —) iron acetate.

time as the decomposition of organic molecules and the formation of CO_2 .

Calcium acetate ($\text{Ca}(\text{CH}_3\text{COO})_2 \cdot \text{H}_2\text{O}$) decomposition takes place in three steps (Fig. 4): 1) the evaporation of water molecules above 200°C , 2) the decomposition of acetate with acetone elimination between 400 and 450°C and 3) the decomposition of CaCO_3 in CaO around 600°C which is in good agreement with the literature [28]. Precursor decomposition temperatures are, then, found in different ranges.

However, two behaviours are identified when iron precursors and calcium acetate are mixed (Fig. 4). For the mixture of iron nitrate and calcium acetate ($\text{FeN}/\text{CaO} (\text{M})$), oxides formation takes place, simultaneously, in a single broad range of temperature between 150 and 500°C because of the complex decomposition of iron nitrate. Two successive ranges are appreciated for the mixture of iron acetate and calcium acetate ($\text{FeAc}/\text{CaO} (\text{M})$): 1) below 400°C , which leads to the formation of iron oxide; 2) around 600°C , which corresponds to the decomposition of the calcium carbonate and the formation of calcium oxide. The decomposition of organic molecules of iron acetate (exothermic) provides energy to shift the decomposition of calcium acetate from 400°C to 350°C . Calcium carbonate decomposes into CaO once iron oxides are produced.

3.1.4. Temperature programmed reduction

The study of iron oxides reducibility (Fig. 5) indicates that the $\text{Ca}_2\text{Fe}_2\text{O}_5$ phase (srebrodolskite), formed by impregnation ($\text{FeAc}/\text{CaO} (\text{I})$) and sol-gel ($\text{FeAc}/\text{CaO} (\text{S})$) syntheses, is reducible into Fe^0 at high temperature (830°C) [25]. Although this phase is not in majority, its reduction can be observed at lower temperatures (775°C and 795°C) for mechanical mixing ($\text{FeAc}/\text{CaO} (\text{M})$ and $\text{FeN}/\text{CaO} (\text{M})$, respectively).

Because the reactivity in toluene steam reforming is efficient in presence of metal iron and is performed at 700°C to be coupled with CO_2 capture, the oxidation state obtained at this temperature is important. The hematite, principally formed by mechanical mixing, is reduced to middle temperatures (450 – 750°C), thus, iron acetate ($\text{FeAc}/\text{CaO} (\text{M})$) leads to the lowest reduction temperature. Then, below 700°C , a large part of the iron oxides can be reduced in Fe^0 in the $\text{FeAc}/\text{CaO} (\text{M})$ material while for $\text{FeN}/\text{CaO} (\text{M})$ the reduction is limited to FeO .

In the other materials, containing a minor hematite phase ($\text{FeAc}/\text{CaO} (\text{I})$ and $\text{FeAc}/\text{CaO} (\text{S})$), magnetite (Fe_3O_4) is the reduced phase at 700°C . This phase could be responsible for a modification

of the selectivity in carbonaceous compounds and in hydrogen due to the Water Gas Shift reaction.

3.2. Textural characterization

3.2.1. Scanning electron microscopy

The scanning electron microscopy allows the determining of the morphology of the materials synthesized by impregnation, sol-gel and mechanical mixing (Fig. 6). Three different structural organizations are observed. The $\text{FeAc}/\text{CaO} (\text{I})$ material (Fig. 6a) comprises of heterogeneous particles of square shape and blades, with an open structure.

The $\text{FeAc}/\text{CaO} (\text{S})$ material (Fig. 6b) shows an open structure composed of particle agglomerates. Contrarily, the material synthesized by mechanical mixing ($\text{FeAc}/\text{CaO} (\text{M})$) has a surface made up of highly dispersed grains distributed (Fig. 6c) so as to form passages between the grains. The pores volume and the surface should be greater than the other two materials.

3.2.2. BET

The results of the surface characterizations of bi-functional materials are presented in Table 4. The BET and pore volume are reported per gram of CaO present in the bi-functional materials. The synthesis method has a weak influence on the specific surface areas of the bi-functional materials (from 6.7 to $10.9 \text{ m}^2/\text{g}_{\text{CaO}}$). However, the values remain lower than those for CaO ($11.3 \text{ m}^2/\text{g}_{\text{CaO}}$).

The bi-functional material prepared by mechanical mixing from iron nitrate ($\text{FeN}/\text{CaO} (\text{M})$) has the largest specific surface area ($10.9 \text{ m}^2/\text{g}_{\text{CaO}}$) and the closest to the corresponding sorbent. It is characterized by the smallest pore size (12.8 nm) and in the field of mesoporous materials.

On the other hand, the bi-functional material prepared by mechanical mixing from iron acetate ($\text{FeAc}/\text{CaO} (\text{M})$) presents the highest pores volume and the closest to the corresponding sorbent.

These results indicate that the synthesis method has an influence on the structural properties of the materials. The differences observed for the pores volume may be explained by the difference in the precursors contact during dissolution for impregnation and sol-gel methods (presence of $\text{Ca}(\text{OH})_2$), compared to the solid state contact for mechanical mixing method. During this step, surface water hydrates the solid mixture and water molecules evaporate in the calcination step where the temperature rate rise is controlled leaving numerous pores. During the calcination, the molecules of calcium acetate and iron acetate become releasing

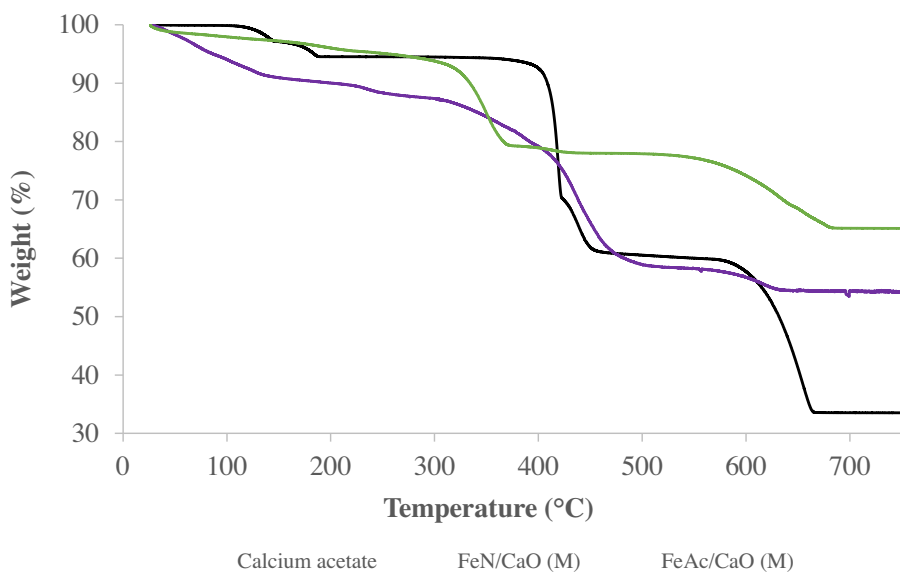


Fig. 4. TGA profiles of (—) calcium acetate, (—) FeAc/CaO (M) and (—) FeN/CaO (M).

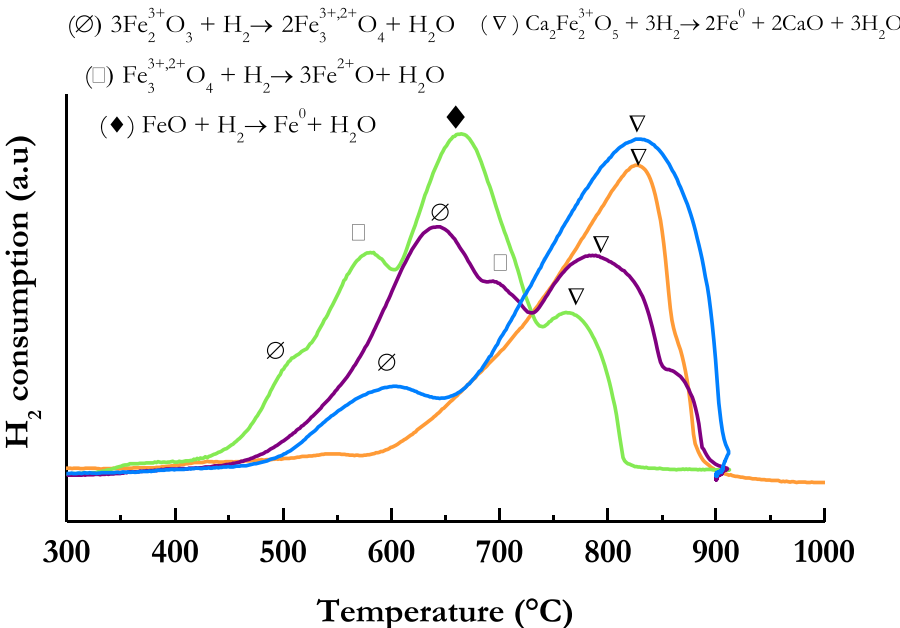


Fig. 5. TPR profiles of bi-functional materials prepared by three synthesis methods (—) FeAc/CaO (I), (—) FeAc/CaO (S), (—) FeAc/CaO (M) also compared to iron nitrate precursor (—) FeN/CaO (M).

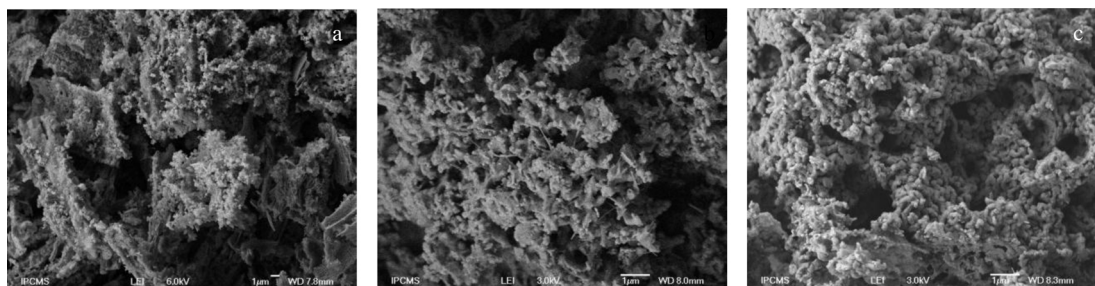


Fig. 6. Micrographs of bi-functional materials synthesized by a) impregnation, b) sol-gel and c) mechanical mixing methods.

organic molecules (acetone, aldehyde) and carbon dioxide favouring the formation of pores. By the pseudo sol-gel method, calcium and iron propionates formation may also promote the forma-

tion of pores during activation. However, results show that this phenomenon is less important than in the mechanical mixing of acetates.

Table 4

Specific surface area, pores volume and mean pores size of the bi-functional materials.

Bi-functional materials	Specific surface area ($\text{m}^2/\text{g}_{\text{CaO}}$)	Pore volume ($\text{cm}^3/\text{g}_{\text{CaO}}$)	Average pore size (nm)
CaO	11.3	5.3×10^{-2}	33.6
FeAc/CaO (I).	8.0	1.9×10^{-2}	42.9
FeAc/CaO (S)	6.7	2.9×10^{-2}	68.7
FeAc/CaO (M)	9.8	7.7×10^{-2}	57.7
FeN/CaO (M)	10.9	3.1×10^{-2}	12.8

3.3. Sorption properties

3.3.1. Sorbent capacity

The sorption tests were performed at 700 °C in a fixed bed reactor. The profiles of the bi-functional materials prepared by the three synthesis methods are compared to the profile of that prepared by mechanical mixing from iron nitrate (Fig. 7). Sorption can be characterized by a rapid carbonation reaction that takes place in the first few seconds. Then, the reaction rate decreases gradually for about 20 min, during which time the layer of CaCO_3 is formed. After that, CO_2 begins its diffusion into the structure. Then, the percentage of CO_2 at the reactor outlet (CO_2 output (%)) is stabilized close to the CO_2 input and the CaO bulk slowly carbonated. Overall, in the sorption sequence both typical mechanisms (kinetic reaction and diffusion controlled) are present.

The carbonation is gradual with FeAc/CaO (I), FeAc/CaO (S) and FeN/CaO (M) bi-functional materials. In the case of FeAc/CaO (M) material, the reaction rate is greater and reaches the stabilization phase, more quickly. The FeAc/CaO (M) surface (Fig. 6c) shows highly dispersed macro grains ($>1 \mu\text{m}$) large enough, according Manovic et al. [29], to discriminate against carbonation. It presents the highest pores volumes (Table 4) that results in a rapid saturation after pores filling due to an easier diffusion during the sorption at 700 °C (Fig. 7).

For the FeAc/CaO (I) and FeAc/CaO (S) materials, these behavioural differences during sorption can also be explained by the scanning electron microscopy observations (Fig. 6). Their surfaces (Fig. 6a and b) show heterogeneous particle agglomeration that forms an open structure. This results in a rapid surface saturation and the formation of a carbonate layer limiting CO_2 diffusion as observed during the sorption at 700 °C (Fig. 7).

The sorption capacity can be expressed as the percentage of the mass of CO_2 captured by the mass of CaO according to Eq. (5):

$$\%C_{\text{CaO}} = \frac{m_{\text{CO}_2}}{m_{\text{CaO}}} \times 100 \quad (5)$$

m_{CO_2} corresponds to the amount (grams) of CO_2 desorbed by the sorbent after sorption at 700 °C and m_{CaO} corresponds to the amount (gram) of CaO in the sample. This latter is measured from the mass of the sample introduced into the reactor, then, corrected due to the percentage of the mass loss observed in TGA analysis reproducing the conditions of the cleaning sequence. The maximum sorption capacity being equimolar, $\%C_{\text{CaO}}$ is about 78%.

According to the results obtained in the fixed bed reactor, the materials with the best sorption properties are those prepared by mechanical mixing (M). This is consistent with the characterization results previously shown. There is a correlation between sorption capacity and specific surface area. The sorption capacity results suggest that granular open structures (Fig. 6a and b) favour the formation of more stable carbonates and the formation of macro grains (Fig. 6c) could reduce the formation of carbonates and preserve CO_2 diffusion.

In the desorption stabilization sequence, CaCO_3 surface decomposition starts at 700 °C, indicating that, either, the CO_2 molecules are loosely bound to the sorbent or that the surface carbonates are not sufficiently stable. During the temperature ramp, CaCO_3 is con-

verted into CaO with the reaction rate increasing with temperature and a maximum desorption temperature (Table 5).

3.3.2. Sorption stability

The sorption capacity values obtained by thermogravimetry (Table 5) were calculated by Eq. (5) where m_{CO_2} corresponds to the gained mass after 1 h of CO_2 sorption at 700 °C and the m_{CaO} to the CaO mass in the sample after each regeneration.

Sorption capacity values obtained by thermogravimetry were much higher than those obtained using the fixed bed (Table 5) and close to the literature values [30,31] and to the theoretical value (78%). The difference is attributed to the experimental conditions; the amount of sample in ATG (about 5 mg) is much lower than that introduced into the fixed bed reactor (100 mg) and, in the latter, diffusion phenomena and mass losses are greater. Due to the high accuracy of the analysis, the thermogravimetry allows the further evaluating of the effect of the texture and the micro structure of the material. Most of the literature's work on the study of CaO sorption capacity is based on thermogravimetric analysis and not on analysis in a fixed bed reactor even if the conditions would be closer to operating conditions.

Sorption capacity is presented as a function of the cycle number (Fig. 8) for sorbent (CaO) and bi-functional materials.

Sorbent (CaO) has a higher initial sorption capacity than materials containing iron. All materials show a decrease in sorption capacity during the 7 sorption-desorption cycles as widely discussed in the literature [32,33]. This is linked to particle agglomeration due to the increase in temperature of the calcination process. When the conversion of CaCO_3 releases CO_2 , gas may remain entrapped within the CaO structure. The presence of CO_2 and the increase in temperature accelerates the sintering phenomenon [34].

A decrease in the specific surface area and pores volume after heat treatment were observed by several authors [35,36] and previously described. According to Alvarez et al. [36], the regeneration of a thin layer of carbonate formed at the CaO surface gives way to the formation of small grains of microporous CaO, which, at the next carbonation, forms a calcium carbonate plug. This is most important when sorption time in the first sorption-desorption cycles is long (30 min) which produces a loss of sorption capacity.

This ageing phenomenon is less noticeable with the FeAc/CaO (I) bi-functional material. Then, the results of sorption and characterizations indicate that the two most promising materials are those prepared by mechanical mixing from iron nitrate or iron acetate using calcium acetate as a precursor of the sorbent phase. In fact, the FeN/CaO (M) an FeAc/CaO (M) bi-functional materials contain $\alpha\text{-Fe}_2\text{O}_3$ phase as the main iron phase, proposed as a precursor of the active phase in steam reforming of tar, reducible at 700 °C (Table 3), have large specific surface area (Table 4) and, good sorption capacity (expressed as $\%C_{\text{CaO}}$) at 700 °C (Table 5) and a carbonation mechanism, that evolves in a limited way in the cycles (Fig. 8). All these characteristics are advantages to using these materials in steam reforming of toluene at 700 °C but catalytic tests are needed to compare them.

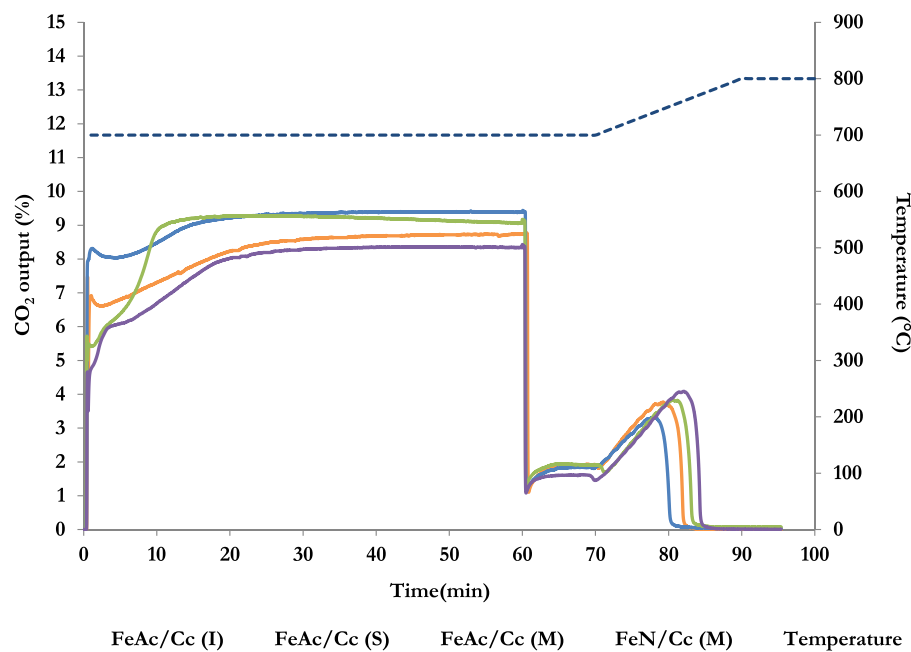


Fig. 7. Sorption-desorption profiles of bi-functional materials (—) FeAc/CaO (I), (—) FeAc/CaO (S), (—) FeAc/CaO (M) also compared to iron nitrate precursor (—) FeN/CaO (M) and (---) temperature ramp.

Table 5

Sorption capacity and desorption temperature obtained in fixed bed reactor and initial sorption capacity obtained by thermo-gravimetric analyses of the sorbent and the bi-functional materials.

Bi-functional materials	Fixed bed reactor		%C _{CaO} at 700 °C
	%C _{CaO} at 700 °C	Maximal desorption temperature (°C)	
CaO	14	765	65
FeAc/CaO (I)	12	740	65
FeAc/CaO (S)	9	735	61
FeAc/CaO (M)	14	750	61
FeN/CaO (M)	16	755	63

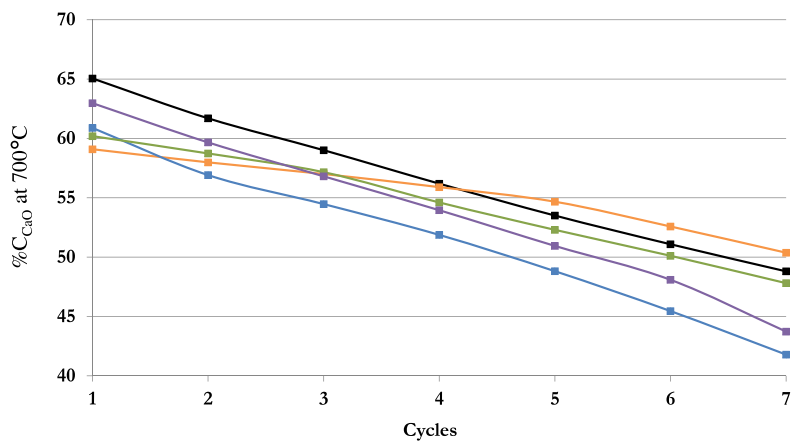


Fig. 8. CO₂ sorption capacity of (—) CaO and bi-functional materials (—) FeAc/CaO (I), (—) FeAc/CaO (S), (—) FeAc/CaO (M) and (—) FeN/CaO (M).

3.4. Catalytic test

Thermodynamically, at temperatures above 500 °C, steam toluene reforming leads to the production of CO, CH₄, CO₂ and H₂ but can also produce benzene by steam dealkylation or hydrodealkylation.

At 700 °C, steam reforming of toluene using FeAc/CaO (I) shows (Fig. 9) the highest hydrogen production rate ($6.1 \times 10^{-3} \text{ mol h}^{-1} \text{ g}^{-1}$) while FeAc/CaO (S) has the lowest activ-

ity after 4 h of reaction ($4.4 \times 10^{-3} \text{ mol h}^{-1} \text{ g}^{-1}$). In both cases Ca₂Fe₂O₅ is mainly present in the samples. The two other materials (M) synthesized by mechanical mixing show appropriate activity and stability over the whole test (around $5.0 \times 10^{-3} \text{ mol h}^{-1} \text{ g}^{-1}$). We can remark that contrary to the three other materials, the activity of FeAc/CaO (M) increases from $3.5 \times 10^{-3} \text{ mol h}^{-1} \text{ g}^{-1}$ to $4.9 \times 10^{-3} \text{ mol h}^{-1} \text{ g}^{-1}$ due to CaO activation.

The CO₂ production rate (Table 6) changes in the same manner as the hydrogen production rate i.e. in a large extent for FeAc/CaO

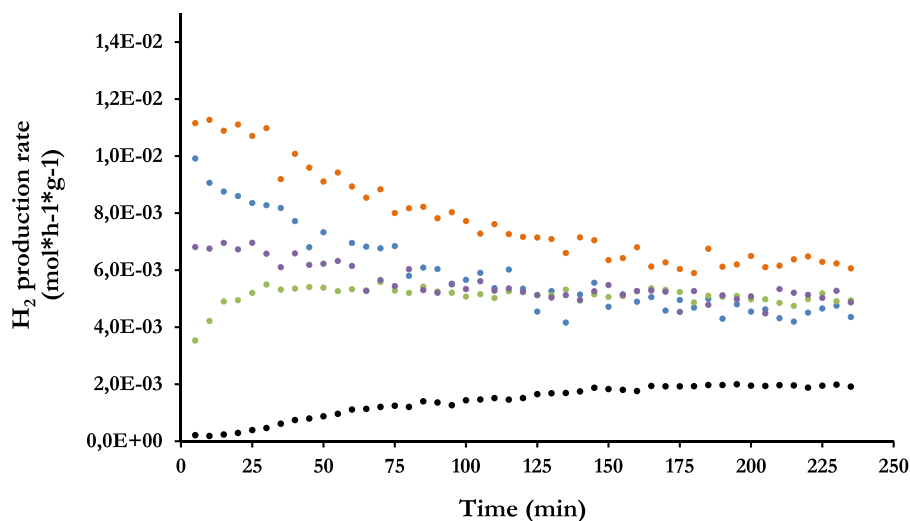


Fig. 9. Hydrogen production rate of (●) CaO and bi-functional materials (○) FeAc/CaO (I), (●) FeAc/CaO (S), (●) FeAc/CaO (M) and (●) FeN/CaO (M).

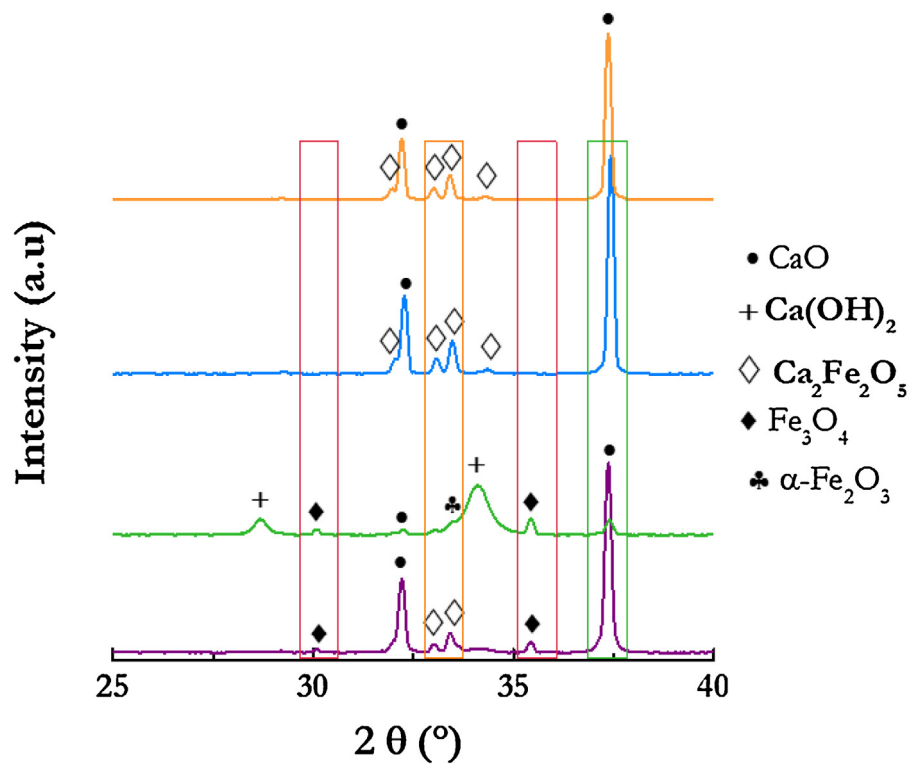


Fig. 10. X-ray diffractograms of bi-functional materials (—) FeAc/CaO (I), (—) FeAc/CaO (S), (—) FeAc/CaO (M) and (—) FeN/CaO (M) after catalytic test.

Table 6

Steam reforming of toluene results: CO₂ production rate and selectivity of CO₂, C₆H₆, and CH₄ at t = 0 and t = 4 h of time on stream.

Bi-functional materials	CO ₂ production rate (mol h ⁻¹ g ⁻¹)		CO ₂ selectivity (%)		C ₆ H ₆ selectivity (%)		CH ₄ selectivity (%)	
	t = 0	t = 4h	t = 0	t = 4h	t = 0	t = 4h	t = 0	t = 4h
CaO	5.4 × 10 ⁻⁵	5.4 × 10 ⁻⁴	45	77	55	23	0	0
FeAc/CaO (I)	3.7 × 10 ⁻³	2.1 × 10 ⁻³	68	68	31	32	1	1
FeAc/CaO (S)	3.4 × 10 ⁻³	1.5 × 10 ⁻³	68	69	31	30	1	1
FeAc/CaO (M)	1.3 × 10 ⁻³	1.6 × 10 ⁻³	58	86	41	13	1	1
FeN/CaO (M)	2.3 × 10 ⁻³	1.6 × 10 ⁻³	55	70	44	29	1	1

(I) and FeAc/CaO (S), and more moderately for FeAc/CaO (M) and FeN/CaO (M). Moreover, the CO₂ production rate is lower than the hydrogen production rate. Under these conditions, the gas mix-

ture is rich in hydrogen (H₂/CO₂ molar ratio around 3 instead of 2.5 theoretically) which means that the bi-functional materials and sorbent are, respectively, effective for hydrogen production by

toluene steam reforming and, at the same time, minimize the CO₂ content in the product gas.

The carbonaceous products (**Table 6**) detected by chromatography are methane with a very low and stable selectivity (%S_{CH4} < 1%), benzene (%S_{C6H6} between 13% and 55%), and carbon dioxide (%S_{CO2} between 45% and 86%). Carbon monoxide is absent, indicating that the Water Gas Shift reaction is enhanced when iron and calcium oxide are present. This suggests that, in the presence of iron, methane production takes place but it is converted by steam reforming or cracking. FeAc/CaO (I) and FeAc/CaO (S) present similar and stable carbonaceous selectivities. On the other hand, FeAc/CaO (M) and FeN/CaO (M) show a decrease in benzene selectivity and an increase in CO₂ selectivity after 4 h.

According to **Fig. 9**, the CaO sorbent is active in toluene steam reforming, which has been already observed by other authors [2] and by our group [37]. However, CaO requires an activation period before promoting hydrogen production and achieving stabilization. This activation step is not detailed in the literature but, generally, it is influenced by the reactions leading to a higher hydrogen production than the simple thermal effect. Taralas et al. [38] used the kinetic model of Langmuir-Hinshelwood to explain the conversion of toluene and hydrogen formation at the CaO surface. Their results suggested that the key step in toluene conversion is the aromatic molecule sorption on the CaO active site. Based on the same model, Simell et al. [39] also suggested that the active site for the benzene steam reforming on dolomite ((Ca,Mg)CO₃) is the Ca²⁺/O²⁻ pair, which allows water and hydrogen sorption. The relationship between toluene and CaO may be governed by the acid-base character. Preferably, toluene is a base through resonant electrons of its aromatic ring. Its pKa (54) [40] is greater than the pKa of CaO (12), the basicity of the latter is provided by the O²⁻ ions. Considering this aspect, toluene which is close to CaO sites have some Lewis acidity which facilitates its conversion into benzene. That explains the presence of benzene (observed with all the studied materials) at the same time as CO₂ and H₂.

In this study, two toluene decomposition pathways can be proposed. The first one consists in the decomposition of toluene to benzene. The O²⁻ oxygen of CaO reacts with hydrogen from the methyl group (sorbed) and forms a phenyl group. The latter, by reaction with CaO, produces CO, hydrogen and a sorbed benzyl that gives benzene [41]. CO is converted by the Water Gas Shift reaction into CO₂, which is finally sorbed by CaO on sites different to those used for toluene conversion. The second toluene decomposition pathway to benzene, methane and/or CO and H₂ can be explained by the breaking up of the H₂ bond at the CaO surface. The sorbed hydrogen may react with toluene to form benzene and sorbed methyl, which desorbs as methane.

CaO sorbent shows high initial benzene selectivity that strongly decreases. An opposite behaviour is observed for CO₂ selectivity that reaches a high value. This suggests that in the first minutes of the reaction, steam dealkylation is more important than toluene steam reforming. Gradually, as the hydrogen production rate increases the selectivity in benzene decreases and that in CO₂ increases. In this way, it can be observed that the progress of the Water Gas Shift reaction enhances the production of CO₂ and H₂, and also shifts the steam reforming reaction.

For the materials synthesized by impregnation (FeAc/CaO (I)) and sol-gel (FeAc/CaO (S)), benzene selectivity is very stable and slightly lower than that obtained with the CaO sorbent. As regards to the materials synthesized by mechanical mixing (FeAc/CaO (M)) and FeN/CaO (M)), variations in benzene selectivity are characterized by a behaviour similar to that of the sorbent (decrease with time).

These results highlight the influence of both Ca₂Fe₂O₅ and Fe₂O₃ iron phases and CaO in the steam reforming of tar and Water Gas Shift reactions. It is apparent that there are two hydrogen produc-

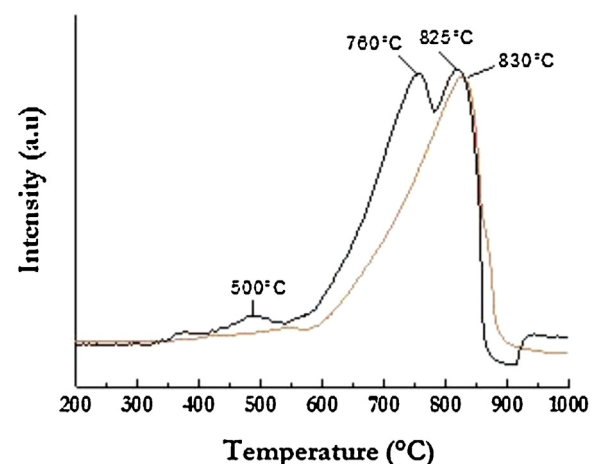


Fig. 11. TPR profiles of bi-functional materials FeAc/CaO(I) (---) before catalytic test and (—) after catalytic test.

tion pathways according to the present iron phase. Ca₂Fe₂O₅ leads to hydrogen production by steam dealkylation and, in the presence of Fe₂O₃, hydrogen is produced by steam reforming and Water Gas Shift reactions. The characterizations, after catalytic test, will clarify these results.

3.5. After test characterizations

Fig. 10 shows the diffractograms of the various bi-functional materials after catalytic test. Materials synthesized by impregnation (FeAc/CaO (I)) and sol-gel (FeAc/CaO (S)) present the major lines of the calcium oxide phase as the corresponding lines of the Ca₂Fe₂O₅ mixed phase. This phase was also identified for these materials by TPR (**Fig. 5**). Apparently, during the catalytic test, there is no formation of a more reduced iron oxide phase (Fe²⁺, Fe⁰). Furthermore, neither carbonate nor calcium hydroxide are detected.

In the case of materials synthesized by mechanical mixing (FeAc/CaO (M) and FeN/CaO (M)), the hematite (α-Fe₂O₃) present in the material before test is transformed during the catalytic test, in magnetite (Fe₃O₄). In the case of FeN/CaO (M), the Ca₂Fe₂O₅ mixed phase is also observed. These results are also in agreement with TPR results (**Fig. 5**). In all cases, the FeO and Fe⁰ phases are absent. Zielinski et al. [42] demonstrated that the reduction of Fe₂O₃ into Fe, in the presence of water and hydrogen, varies with the H₂O/H₂ ratio. Under the conditions of the tests carried out in this work, the amount of water is greater than that of H₂, which explains the absence of the strongly reduced phases such as FeO or Fe⁰ and the main presence of the Fe₃O₄ phase.

Characterisations by TPR and Mossbauer spectroscopy, performed after catalytic test, allow the understanding of the iron species reduction during catalytic test.

The TPR results (**Fig. 11**) suggest that the consumption of hydrogen, around 830 °C, corresponds to the reduction of Fe³⁺ of the Ca₂Fe₂O₅ phase (srebrodolskite). This latter is reorganized under reforming conditions by modification of Fe-Ca interactions (reduction centred around 825 °C). Iron species (such as α-Fe₂O₃ form) are more available for reduction as observed between 500 °C and 760 °C.

The presence of this phase (α-Fe₂O₃), not observed by XRD but highlighted by TPR, was confirmed by Mossbauer spectroscopy (**Table 7**). This may be explained by the structural characteristics of the srebrodolskite phase and by the conditions of steam reforming involved in this structure modification. The activity of all the studied materials is similar after stabilization because of the simultaneous presence of Fe³⁺ in Ca₂Fe₂O₅ and Fe³⁺ in Fe₂O₃.

Table 7

Iron distribution in the bi-functional material FeAc/CaO (I) by Mossbauer spectroscopy.

FeAc/CaO(I)	$\text{Ca}_2\text{Fe}_2\text{O}_5$	Fe_2O_3
Before test	94%	6%
After test	88%	12%

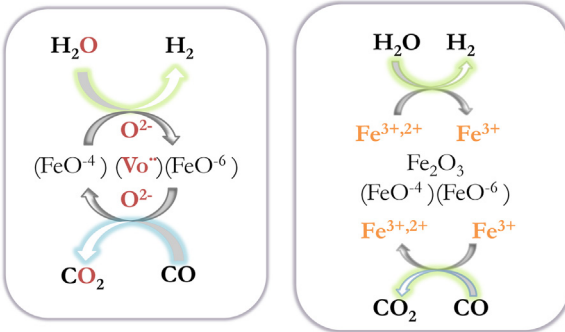


Fig. 12. Evolution of the $\text{Ca}_2\text{Fe}_2\text{O}_5$ phase during toluene steam reforming (FeO^{4-} -tetrahedron and FeO^{-6} -octahedron, Vo° = oxygen vacancies) (left). Reaction mechanism of hematite Fe_2O_3 during steam reforming of toluene (right).

In the presence of the mixed phase $\text{Ca}_2\text{Fe}_2\text{O}_5$ and the dispersed paramagnetic phase (Fe_2O_3), the hydrogen production rate is greater than that observed with CaO sorbent. This suggests that the presence of $\text{Ca}_2\text{Fe}_2\text{O}_5$ contributes to the catalytic activity of Fe/CaO system. The stability of the CO_2 selectivity could be the result of the mixed phase ($\text{Ca}_2\text{Fe}_2\text{O}_5$) activity in the Water Gas Shift reaction and better availability of active sites in the CaO for the capture of CO_2 .

In the presence of the hematite phase (α - Fe_2O_3), the selectivity to CO_2 increases at the same time that the benzene selectivity decreases. According to these results, the iron oxide promotes the breaking of the C–C and C–H bonds of organic molecules and the CO produced is oxidized to CO_2 by iron oxide reduction, which indicates that the Water Gas Shift reaction is enhanced.

Then, in the presence of iron element, the hydrogen production mechanism depends on the iron oxide phase. The evolution of the Water Gas Shift reaction in the presence of $\text{Ca}_2\text{Fe}_2\text{O}_5$ can be explained by the following mechanism. The oxygen vacancies of the $\text{Ca}_2\text{Fe}_2\text{O}_5$ structure favour the reduction of water (Fig. 12 left), and $\text{Ca}_2\text{Fe}_2\text{O}_5$ reorganizes by releasing oxygen which oxidizes CO to CO_2 .

When Fe_2O_3 is present, the Water Gas Shift reaction borrows the following mechanism (Fig. 12 right). Fe^{3+} is reduced to $\text{Fe}^{3+,2+}$ by the hydrogen produced during toluene steam reforming in the presence of CaO . Then, Fe_3O_4 allows the reduction of water into H_2 . The Fe_2O_3 reduction allows the oxidation of CO to CO_2 [43].

4. Conclusion

The results suggest that the activity of Fe/CaO materials depends not only on the presence of Fe_2O_3 but also on the stability of the interactions between iron and calcium under reaction conditions. According to the sorption capacity and stability and catalytic activity results, FeAc/CaO (I) and FeAc/CaO (M) are promising bi-functional materials for CO_2 capture and tar steam reforming. In fact, FeAc/CaO (M) presents the appropriate properties (large specific surface area, appropriate sorption capacity at 700°C , and the lowest deactivation) for CO_2 capture. This material also contains α - Fe_2O_3 phase, the precursor of the active phase in steam reforming of tar, reducible at 700°C . For its part, FeAc/CaO (I) structure evolves under reac-

tion conditions that permit the increasing of Fe_2O_3 content in the sample during reactivity tests.

Finally, the bi-functional material prepared from iron acetate and calcium acetate by mechanical mixing (FeAc/CaO (M)) has a stable activity over time, and a CO_2 selectivity that indicates that the Water Gas Shift reaction is important. In addition, it has a lower benzene selectivity than other materials due to its higher availability of iron (Fe_2O_3) for steam toluene reforming and C–C breaking.

Acknowledgements

We acknowledge the National Center of Scientific Research (CNRS) and Alsace region for the financial support to carry out this work. Authors also express our gratitude to Daniel Schwartz for his help in improving the standard of English of this paper.

References

- [1] M. Widywati, T.L. Church, N.H. Florin, A.T. Harris, Hydrogen synthesis from biomass pyrolysis with in situ carbon dioxide capture using calcium oxide, Int. J. Hydrogen Energy 36 (2011) 4800–4813, <http://dx.doi.org/10.1016/j.ijhydene.2010.11.103>.
- [2] J. Delgado, M.P. Aznar, J. Corella, Biomass gasification with steam in fluidized bed: effectiveness of CaO , MgO , and $\text{CaO}-\text{MgO}$ for hot raw gas cleaning, Ind. Eng. Chem. Res. 36 (1997) 1535–1543, <http://dx.doi.org/10.1021/ie960273w>.
- [3] L. Devi, K.J. Ptasinski, F.J.J.G. Janssen, S.V.B. van Paasen, P.C.A. Bergman, J.H.A. Kiel, Catalytic decomposition of biomass tars: use of dolomite and untreated olivine, Renew. Energy 30 (2005) 565–587, <http://dx.doi.org/10.1016/j.renene.2004.07.014>.
- [4] D. Świarczyński, S. Libs, C. Courson, A. Kiennemann, Steam reforming of tar from a biomass gasification process over Ni/olivine catalyst using toluene as a model compound, Appl. Catal. B: Environ. 74 (2007) 211–222, <http://dx.doi.org/10.1016/j.apcatb.2007.01.017>.
- [5] M. Virginie, C. Courson, D. Niznansky, N. Chaoui, A. Kiennemann, Characterization and reactivity in toluene reforming of a Fe/olivine catalyst designed for gas cleanup in biomass gasification, Appl. Catal. B: Environ. 101 (2010) 90–100, <http://dx.doi.org/10.1016/j.apcatb.2010.09.011>.
- [6] L. Di Felice, C. Courson, D. Niznansky, P.U. Foscolo, A. Kiennemann, Biomass gasification with catalytic tar reforming: a model study into activity enhancement of calcium- and magnesium-oxide-based catalytic materials by incorporation of iron, Energy Fuels 24 (2010) 4034–4045, <http://dx.doi.org/10.1021/ef100351j>.
- [7] Z. Min, M. Asadullah, P. Yimsiri, S. Zhang, H. Wu, C.-Z. Li, Catalytic reforming of tar during gasification. Part I. Steam reforming of biomass tar using ilmenite as a catalyst, Fuel 90 (2011) 1847–1854, <http://dx.doi.org/10.1016/j.fuel.2010.12.039>.
- [8] L. Dong, M. Asadullah, S. Zhang, X.-S. Wang, H. Wu, C.-Z. Li, An advanced biomass gasification technology with integrated catalytic hot gas cleaning Part I. Technology and initial experimental results in a lab-scale facility, Fuel 108 (2013) 409–416, <http://dx.doi.org/10.1016/j.fuel.2012.11.043>.
- [9] M. Koike, D. Li, H. Watanabe, Y. Nakagawa, K. Tomishige, Comparative study on steam reforming of model aromatic compounds of biomass tar over Ni and Ni–Fe alloy nanoparticles, Appl. Catal. A: Gen. 506 (2015) 151–162, <http://dx.doi.org/10.1016/j.apcata.2015.09.007>.
- [10] S.S. Tamhankar, K. Tsuchiya, J.B. Riggs, Catalytic cracking of benzene on iron oxide–silica: catalyst activity and reaction mechanism, Appl. Catal. 16 (1985) 103–121, [http://dx.doi.org/10.1016/S0166-9834\(00\)84073-7](http://dx.doi.org/10.1016/S0166-9834(00)84073-7).
- [11] T. Nordgreen, T. Liliedahl, K. Sjöström, Metallic iron as a tar breakdown catalyst related to atmospheric, fluidised bed gasification of biomass, Fuel 85 (2006) 689–694, <http://dx.doi.org/10.1016/j.fuel.2005.08.026>.
- [12] M. Virginie, J. Adánez, C. Courson, L.F. De Diego, F. García-Labiano, D. Niznansky, A. Kiennemann, P. Gayan, A. Abad, Effect of Fe-olivine on the tar content during biomass gasification in a dual fluidized bed, Appl. Catal. B: Environ. 121–122 (2012) 214–222, <http://dx.doi.org/10.1016/j.apcatb.2012.04.005>.
- [13] C. Ratnasamy, J.P. Wagner, Water gas shift catalysis, Catal. Rev. 51 (3) (2009) 325–440, <http://dx.doi.org/10.1080/01614940903048661>.
- [14] M.A. Uddin, H. Tsuda, S. Wu, E. Sasaoka, Catalytic decomposition of biomass tars with iron oxide catalysts, Fuel 87 (2008) 451–459, <http://dx.doi.org/10.1016/j.fuel.2007.06.021>.
- [15] S. Lin, M. Harada, Y. Suzuki, H. Hatano, Hydrogen production from coal by separating carbon dioxide during gasification, Fuel 81 (2002) 2079–2085, [http://dx.doi.org/10.1016/S0016-2361\(02\)00187-4](http://dx.doi.org/10.1016/S0016-2361(02)00187-4).
- [16] H. Lu, E.P. Reddy, P.G. Smirniotis, Calcium oxide based sorbents for capture of carbon dioxide at high temperatures, Ind. Eng. Chem. Res. 45 (2006) 3944–3949, <http://dx.doi.org/10.1021/ie051325x>.
- [17] B.S. Huang, H.Y. Chen, K.H. Chuang, R.X. Yang, M.Y. Wey, Hydrogen production by biomass gasification in a fluidized bed reactor promoted by an Fe/CaO catalyst, Int. J. Hydrogen Energy 37 (2012) 6511–6518, <http://dx.doi.org/10.1016/j.ijhydene.2012.01.071>.

- [18] J. Berggren, Refinement of the crystal structure of dicalcium ferrite, $\text{Ca}_2\text{Fe}_2\text{O}_5$, *Acta Chem. Scand.* 25 (1971) 3616–3624.
- [19] J.C. Grenier, M. Pouchard, P. Hagenmuller, Vacancy ordering in oxygen-deficient perovskite related ferrites, *Struct. Bond.* 47 (1981) 1–25.
- [20] N.L. Ross, R.J. Angel, F. Seifert, Compressibility of Brownmillerite ($\text{Ca}_2\text{Fe}_2\text{O}_5$): effect of vacancies on the elastic properties of perovskites, *Phys. Earth Planet. Inter.* 129 (2002) 145–151, [http://dx.doi.org/10.1016/S0031-9201\(01\)00269-2](http://dx.doi.org/10.1016/S0031-9201(01)00269-2).
- [21] L.A. Isupova, S.V. Tsybulya, G.N. Kryukova, A.A. Budneva, E.A. Paukshtis, G.S. Litvak, V.P. Ivanov, V.N. Kolomichuk, Y.T. Pavlyukhin, V.A. Sadykov, Mechanochemical synthesis and catalytic properties of the calcium ferrite $\text{Ca}_2\text{Fe}_2\text{O}_5$, *Kinet. Catal.* 43 (2002) 122–128, <http://dx.doi.org/10.1023/A:1014217716883>.
- [22] D. Hirabayashi, T. Yoshikawa, K. Mochizuki, K. Suzuki, Y. Sakai, Formation of Brownmillerite type calcium ferrite ($\text{Ca}_2\text{Fe}_2\text{O}_5$) and catalytic properties in propylene combustion, *Catal. Lett.* 110 (2006) 269–274, <http://dx.doi.org/10.1007/s10562-006-0120-0>.
- [23] S. Shin, Y. Hatakeyama, K. Ogawa, K. Shimomura, Catalytic decomposition of nitric oxide over Brownmillerite-like compounds, calcium ferrate (III) ($\text{Ca}_2\text{Fe}_2\text{O}_5$) and strontium ferrate (III) ($\text{Sr}_2\text{Fe}_2\text{O}_5$), *Mat. Res. Bull.* 14 (1979) 133–136, [http://dx.doi.org/10.1016/0025-5408\(79\)90241-1](http://dx.doi.org/10.1016/0025-5408(79)90241-1).
- [24] F. Garcia-Labiano, A. Abad, L.F. de Diego, P. Gayan, J. Adanez, Calcination of calcium-based sorbents at pressure in a broad range of CO_2 concentrations, *Chem. Eng. Sci.* 57 (2002) 2381–2393, [http://dx.doi.org/10.1016/S0009-2509\(02\)00137-9](http://dx.doi.org/10.1016/S0009-2509(02)00137-9).
- [25] I. Zamboni, C. Courson, A. Kienemann, Synthesis of Fe/CaO active sorbent for CO_2 absorption and tars removal in biomass gasification, *Catal. Today* 176 (2011) 197–201, <http://dx.doi.org/10.1016/j.cattod.2011.01.014>.
- [26] M.D. Brown, E.G. Baker, L.K. Mudge, Environmental design considerations for thermochemical biomass energy, *Biomass* 11 (1986) 255–270, [http://dx.doi.org/10.1016/0144-4565\(86\)90098-3](http://dx.doi.org/10.1016/0144-4565(86)90098-3).
- [27] K. Wieczorek-Ciurowa, A.J. Kozak, The thermal decomposition of $\text{Fe}(\text{NO}_3)_3 \times 9\text{H}_2\text{O}$, *J. Therm. Anal. Calorim.* 58 (1999) 647–651, <http://dx.doi.org/10.1023/A:1010112814013>.
- [28] J. Adanez, L.F. de Diego, F. Garcia-Labiano, Calcination of calcium acetate and calcium magnesium acetate: effect of the reacting atmosphere, *Fuel* 78 (1999) 583–592, [http://dx.doi.org/10.1016/S0016-2361\(98\)00186-0](http://dx.doi.org/10.1016/S0016-2361(98)00186-0).
- [29] V. Manovic, E.J. Anthony, Long-term behavior of CaO-based pellets supported by calcium aluminate cements in a long series of CO_2 capture cycles, *Ind. Eng. Chem. Res.* 48 (2009) 8906–8912, <http://dx.doi.org/10.1021/ie9011529>.
- [30] H. Guo, S. Wang, C. Li, Y. Zhao, Q. Sun, X. Ma, Incorporation of Zr into calcium oxide for CO_2 capture by a simple and facile sol-gel method, *Ind. Eng. Chem. Res.* 55 (2016) 7873–7879, <http://dx.doi.org/10.1021/acs.iecr.5b04112>.
- [31] M.S. Yancheshmeh, H.R. Radfarnia, M.C. Iliuta, High temperature CO_2 sorbents and their application for hydrogen production by sorption enhanced steam reforming process, *Chem. Eng. J.* 283 (2016) 420–444, <http://dx.doi.org/10.1016/j.cej.2015.06.060>.
- [32] G. Grasa, B. González, M. Alonso, J.C. Abanades, Comparison of CaO-based synthetic CO_2 sorbents under realistic calcination conditions, *Energ. Fuel.* 21 (2007) 3560–3562, <http://dx.doi.org/10.1021/ef0701687>.
- [33] J.C. Abanades, The maximum capture efficiency of CO_2 using a carbonation/calcination cycle of CaO/CaCO_3 , *Chem. Eng. J.* 90 (2002) 303–306, [http://dx.doi.org/10.1016/S1385-8947\(02\)00126-2](http://dx.doi.org/10.1016/S1385-8947(02)00126-2).
- [34] R.H. Borgwardt, N.F. Roache, K.R. Bruce, Method for variation of grain size in studies of gas-solid reactions involving calcium oxide, *Ind. Eng. Chem. Fund.* 25 (1986) 165–169, <http://dx.doi.org/10.1021/i100021a026>.
- [35] R.H. Borgwardt, Calcium oxide sintering in atmospheres containing water and carbon dioxide, *Ind. Eng. Chem. Res.* 28 (1989) 493–500, <http://dx.doi.org/10.1021/ie00088a019>.
- [36] D. Alvarez, J.C. Abanades, Pore-size and shape effects on the recarbonation performance of calcium oxide submitted to repeated calcination/recarbonation cycles, *Energ. Fuel.* 19 (2005) 270–278, <http://dx.doi.org/10.1021/ef049864m>.
- [37] I. Zamboni, C. Courson, D. Niznansky, A. Kienemann, Simultaneous catalytic H_2 production and CO_2 capture in steam reforming of toluene as tar model compound from biomass gasification, *Appl. Catal. B: Environ.* 145 (2014) 63–72, <http://dx.doi.org/10.1016/j.apcatb.2013.02.046>.
- [38] G. Taralas, M.G. Kontominas, Kinetic modelling of VOC catalytic steam pyrolysis for tar abatement phenomena in gasification/pyrolysis technologies, *Fuel* 83 (2004) 1235–1245, <http://dx.doi.org/10.1016/j.fuel.2003.11.010>.
- [39] P.A. Simell, E.K. Hirvensalo, V.T. Smolander, A.O.I. Krause, Steam reforming of gasification gas tar over dolomite with benzene as a model compound, *Ind. Eng. Chem. Res.* 38 (1999) 1250–1257, <http://dx.doi.org/10.1021/ie980646o>.
- [40] B.A. Sim, D. Griller, D.D.M. Wayner, Reduction potentials for substituted benzyl radicals: pKa values for the corresponding toluenes, *J. Am. Chem. Soc.* 111 (1989) 754–755, <http://dx.doi.org/10.1021/ja00184a066>.
- [41] C.K.S. Lai, Thesis: thermal reactions of aromatic hydrocarbons and n-cresol over calcium oxide, Massachusetts Institute of Technology, Dept. Chem. Eng. (1986) <http://hdl.handle.net/1721.1/15044>.
- [42] J. Zieliński, I. Zglinicka, L. Znak, Z. Kaszkur, Reduction of Fe_2O_3 with hydrogen, *Appl. Catal. A-Gen.* 381 (2010) 191–196, <http://dx.doi.org/10.1016/j.apcata.2010.04.003>.
- [43] E. de Smit, B.M. Weckhuysen, The renaissance of iron-based Fischer-Tropsch synthesis: on the multifaceted catalyst deactivation behaviour, *Chem. Soc. Rev.* 37 (2008) 2758–2781, <http://dx.doi.org/10.1039/b805427d>.